Built-in Electric Field Induces High-Performance Hydrogen Evolution Reaction on a Self-Supporting MoO_2-NiP/NF Heterojunction

Chunhui Bai,[a] Yu Shen,[a] Feng Yan,*[a] Qiuye Wang,[b] Bo Geng,[c] Chunling Zhu*[b] and Yujin Chen*[a]

[a] Key Laboratory of In-Fiber Integrated Optics, Ministry of Education, College of Physics and Optoelectronic Engineering, Harbin Engineering University, Harbin 150001, China. E-mail: yanfeng@hrbeu.edu.cn; chenyujin@hrbeu.edu.cn

[b] Key Laboratory of Superlight Materials and Surface Technology, Ministry of Education, College of Chemistry and Chemical Engineering, Harbin Engineering University, Harbin 150001, China. E-mail: zhuchunling@hrbeu.edu.cn

[c] School of Physics and Engineering, Henan University of Science and Technology, Luoyang 471023, China.

Experimental method

Materials： All chemical reagents were of analytical reagent grade and used without further purification. Specifically, nickel nitrate hexahydrate ($Ni(NO_3)_2·6H_2O$) and commercial 20 wt% platinum on carbon (Pt/C) were procured from Tianjin Guangfu Fine Chemical Research Institute. Hydrochloric acid (HCl), ammonium molybdate tetrahydrate ($(NH_4)_6Mo_7O_{24}·4H_2O$), and sodium hypophosphite monohydrate ($NaH_2PO_2·H_2O$) were obtained from Shanghai Aladdin biochemical technology co., LTD.

The processing of NF precursors

Following a reported procedure, the nickel mesh (3 cm*3 cm) was initially ultrasonically cleaned in a 3:1 mixture of HCl and deionized water (20 mL HCl: 60 mL H_2O) for 15 minutes. It was subsequently rinsed sequentially with 50 mL of deionized water and 50 mL of absolute ethanol under ultrasonication for 10 minutes each. Finally, the sample was thoroughly washed with deionized water and ethanol, and then dried overnight in a vacuum oven at 90°C.

Synthesis of $NiMoO_4$/NF

$NiMoO_4$ nanostructures were grown in situon nickel foam (NF) via a facile hydrothermal method. In a typical synthesis, 0.9 g of $Ni(NO_3)_3 \cdot 6H_2O$ and 0.31 g of $(NH_4)_6$ $Mo_7O_{24} \cdot 4H_2O$ were dissolved in 40 mL of deionized water under constant magnetic stirring for 30 minutes. The homogeneous solution was then transferred into a 50 mL Teflon-lined stainless steel autoclave, sealed, and maintained at 160°C for 6 hours in an electric oven. After the autoclave was allowed to cool naturally to ambient temperature, the resulting $NiMoO_4$/NF electrode was removed, rinsed thoroughly with deionized water and ethanol to remove any loosely adsorbed species, and finally dried overnight at 90°C in a vacuum oven.

MoO_2-NiP/NF-400

MoO_2-NiP/NF-400 was synthesized via phosphidation process. The $NiMoO_4$/NF precursor and NaH_2PO_2 (phosphorus source) were loaded into two separate ceramic boats, with NaH_2PO_2 positioned upstream in a tube furnace. Under a continuous argon flow, the temperature was raised to 400°C at a rate of 5°C min^{-1} and held for 3 h. After naturally cooling to room temperature under argon, the final product, denoted as MoO_2-NiP/NF-400, was collected for further use.

MoO_2-NiP/NF-300 and MoO_2-NiP/NF-500

Following the aforementioned procedure, the heating temperature was increased to 300°C and subsequently to 500°C.

Structural characterization

The crystal phase composition of the as-synthesized materials was determined by X-ray diffraction (XRD) on a Panalytical X'pert diffractometer using Cu Kα radiation (λ=1.5418 Å). Morphological and structural analyses were performed using a Hitachi SU70 scanning electron microscope (SEM) and an FEI Tecnai-F20 transmission electron microscope (TEM). The surface elemental composition and chemical states were characterized by X-ray photoelectron spectroscopy (XPS) on a Thermo Fisher Scientific instrument with an Al Kα source.

Electrochemical testing

All electrochemical measurements for the hydrogen evolution reaction (HER) were performed at room temperature in 1 M KOH using a standard three-electrode system on a CHI760E electrochemical workstation. The self-supporting MoO_2-NiP/NF was used directly as the working electrode with a geometric area of 1 cm^2, without any

binder or conductive additives. A saturated Hg/HgO electrode and a graphite rod served as the reference and counter electrodes, respectively. For comparison, 20 wt% Pt/C and IrO_2 electrodes were prepared by coating a uniform catalyst ink onto nickel foam. The ink was formulated by ultrasonically dispersing 8 mg of catalyst powder in a mixture of 1 mL ethanol and 40 uL Nafion solution for 30 min, resulting in a catalyst loading of approximately 2 mg cm^{-2}.

The HER activity was evaluated from polarization curves obtained via linear sweep voltammetry (LSV) at a scan rate of 5 mV s^{-1}. The corresponding Tafel slopes were calculated by fitting the data to the Tafel equation ($\eta = a + b \log|j|$). The electrochemical double-layer capacitance (C_{dl}) was estimated from cyclic voltammetry measurements within a non-Faradaic potential window (0.75 ~ 0.85 V vs. RHE) at scan rates varying from 100 to 180 mV s^{-1}. Electrochemical impedance spectroscopy (EIS) was performed over a frequency range of 0.01 Hz to 100 kHz. Long-term stability was assessed by chronopotentiometry. All reported potentials were converted to the reversible hydrogen electrode (RHE) scale using the equation $E_{RHE} = E_{Hg/HgO} + 0.059 \times pH + 0.098$ V, and the LSV data were *iR*-compensated post-measurement using $E_{compensated} = E_{measured} - iR$, where $E_{measured}$ is the experimentally measured potential and $E_{compensated}$ is the *iR*-compensated potential, and R represents the uncompensated solution resistance determined by the current interruption method.

TOF Calculation

The turnover frequency (TOF) per active site was determined as follow. First, cyclic voltammetry was performed in phosphate buffer (pH = 7) at a scan rate of 50 mV s^{-1} (potential range: -0.2 ~0.8 V *vs.* RHE) to quantify the number of active sites. The Faradaic charge was obtained after subtracting the background current. The number of active sites for the hydrogen evolution reaction, n(mol), and the TOF (s^{-1}) were then calculated using the following equations:

$$n = Q \,/\, 2F$$

$$TOF = j \,/\, 2Fn$$

where j denotes the measured current density and F is the Faraday constant (96485.3 C mol^{-1}).

Membrane electrode assemblies were fabricated using IrO_2/NF as the anode and Pt/C/NF or MoO_2-NiP/NF-400 as the cathode, respectively. Their electrochemical performance was evaluated and compared by linear sweep voltammetry in 1 M KOH at a scan rate of 5 $mV \cdot s^{-1}$.

Calculation Details

All DFT calculations were performed using the CASTEP module in Materials Studio. The calculations covered the density of states (DOS), charge density difference, and adsorption energies. The Perdew-Burke-Ernzerhof (PBE) functional within the generalized gradient approximation (GGA) was employed to describe the exchange-correlation effects. A plane-wave energy cutoff of 400 eV was adopted for all structural relaxations, energy calculations, and electronic property analyses. A vacuum layer of 15 Å was introduced along the z direction to avoid spurious interactions between periodic images. The Brillouin zone was sampled using a 2 × 2 × 1 Monkhorst-Pack k-point grid.

The water adsorption energies (ΔE_{H2O}) at the sample of surfaces were calculated by the equation of $\Delta E_{(H2O)} = E_{surf+H2O} - E_{surf} - E_{H2O}$, where the E_{surf} and the $E_{surf+H2O}$ are the total energies of the surface before and after water adsorption, and E_{H2O} is the energy of a free water. The Gibbs free energies for hydrogen adsorption (ΔG_{H*}) were calculated from the equation: $\Delta G_{H*} = \Delta E_{H*} + \Delta ZPE - T\Delta S$, where the ΔE_{H*}, ΔZPE, T, and ΔS represent the binding energy, zero point energy change, temperature, and entropy change of H* adsorption system, respectively. As the entropy of hydrogen in absorbed state is negligible, ΔS can be calculated as -1/2 S_0 (S_0 is the entropy of H_2 in the gas phase at standard conditions, 1 bar of H_2 and pH = 0 at 300 K).

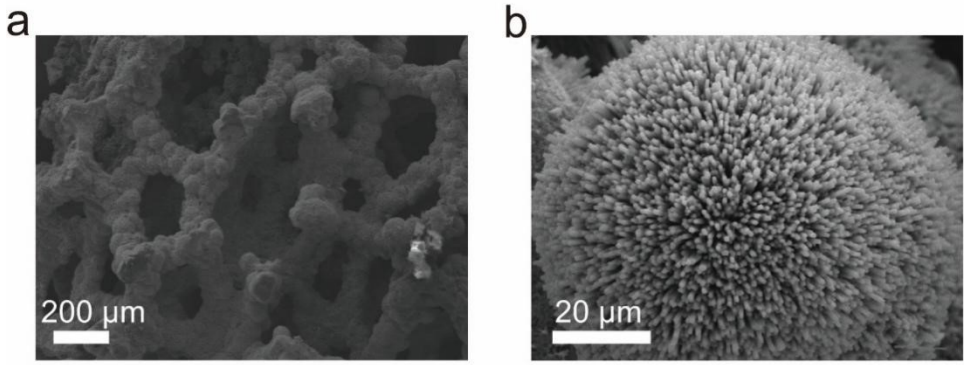

Figure S1. SEM images of (a,b) MoO_2-NiP/NF-400.

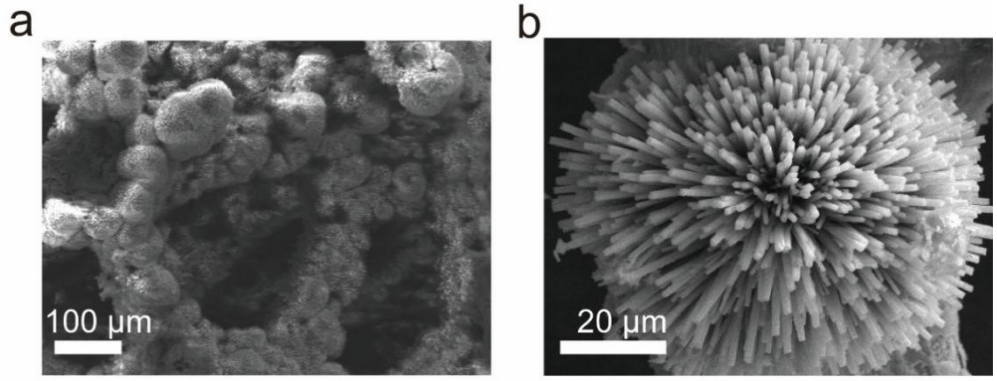

Figure S2. SEM images of (a,b) MoO_2-NiP/NF-300.

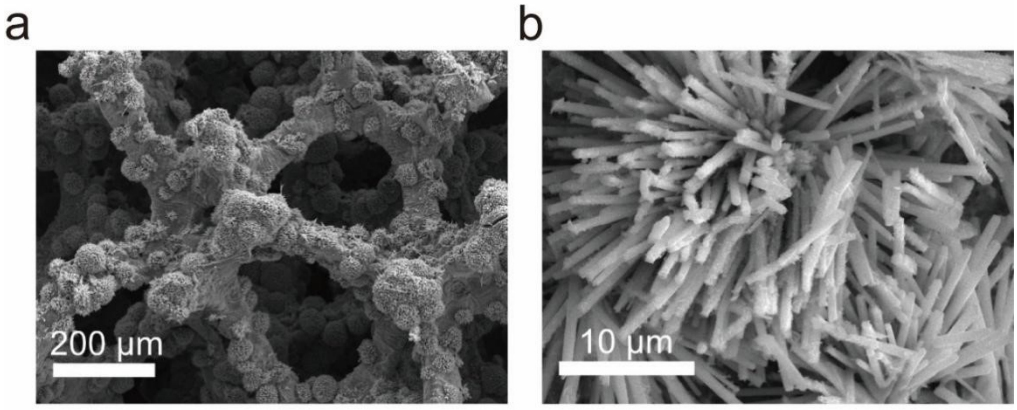

Figure S3. SEM images of (a,b) MoO_2-NiP/NF-500.

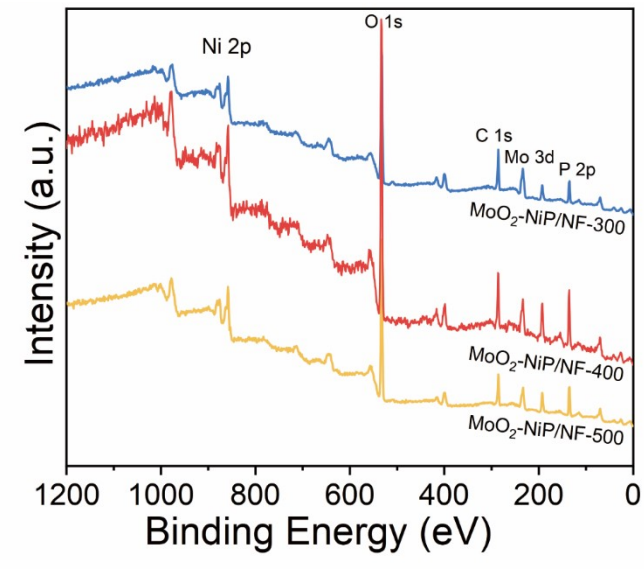

Figure S4. Survey XPS spectra of MoO_2-NiP/NF-300, MoO_2-NiP/NF-400, and MoO_2-NiP/NF-500.

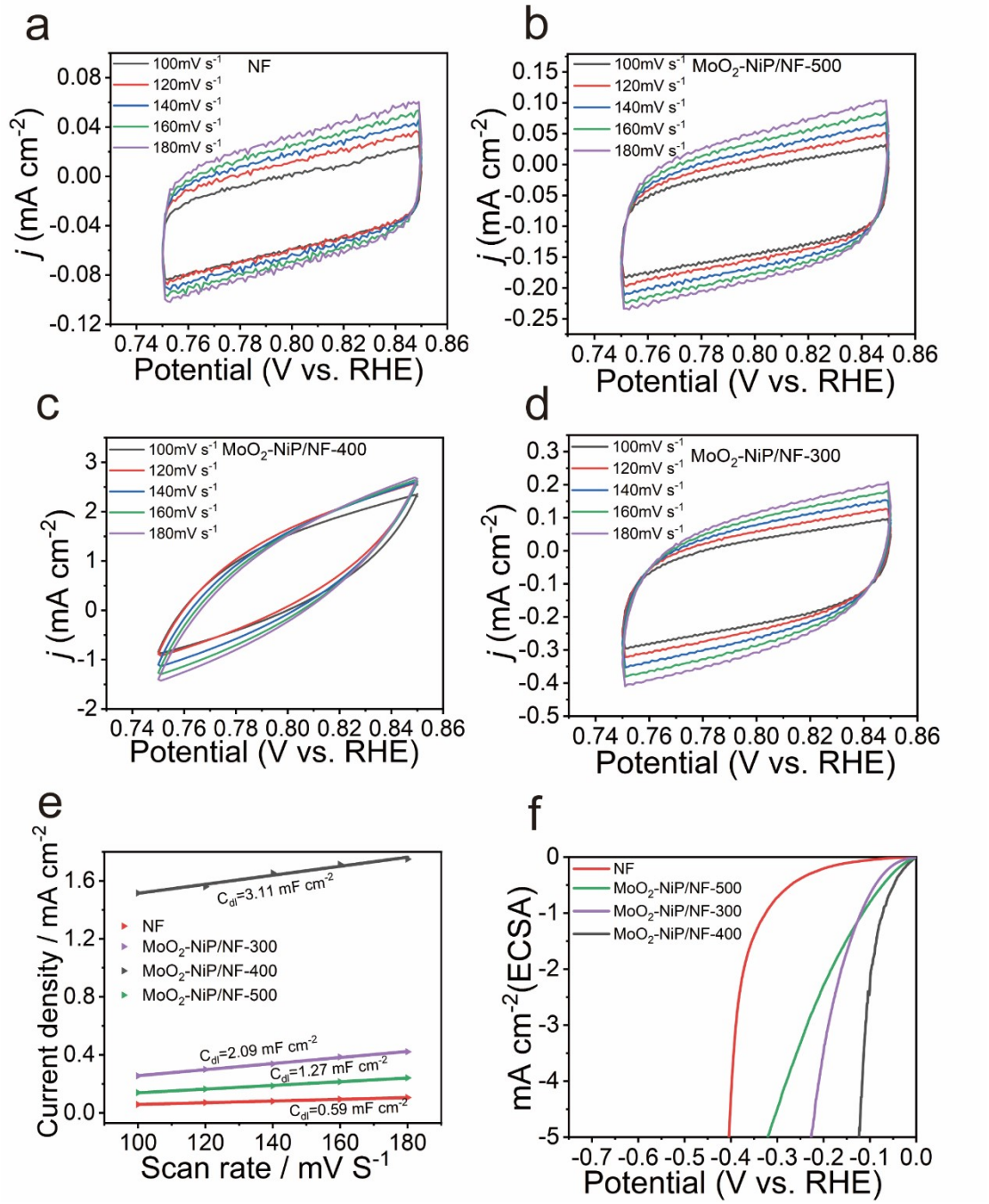

Figure S5. CV curves of (a) NF, (b) MoO_2-NiP/NF-500, (c) MoO_2-NiP/NF-400, and (d) MoO_2-NiP/NF-300 at scan rates from 100 to 180 mV s^{-1} in 1 M KOH. (e) The double-layer capacitance (C_{dl}) values for NF, MoO_2-NiP/NF-500, MoO_2-NiP/NF-400, and MoO_2-NiP/NF-300. (f) ECSA-normalized HER polarization curves of different catalysts.

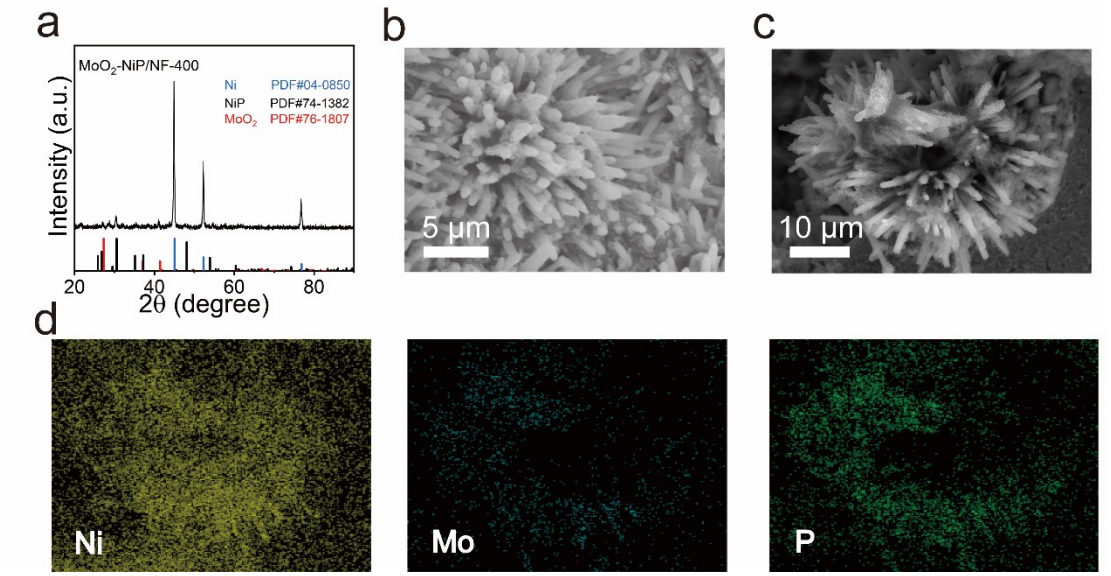

Figure S6. (a) XRD pattern of MoO_2-NiP/NF-400 after HER testing. (b, c) SEM images and (d) EDS elemental mapping of MoO_2-NiP/NF-400 after HER testing.

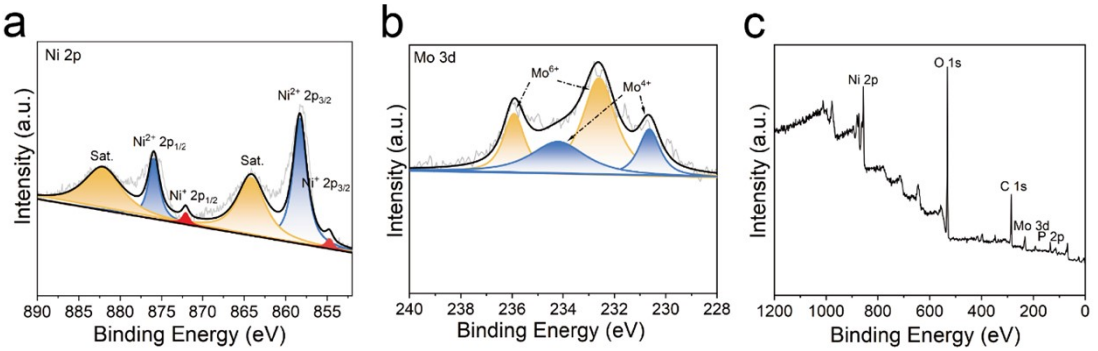

Figure S7. XPS spectra of (a) Ni 2p, (b) Mo 3d, and (c) survey spectrum for MoO_2-NiP/NF-400 after HER testing.

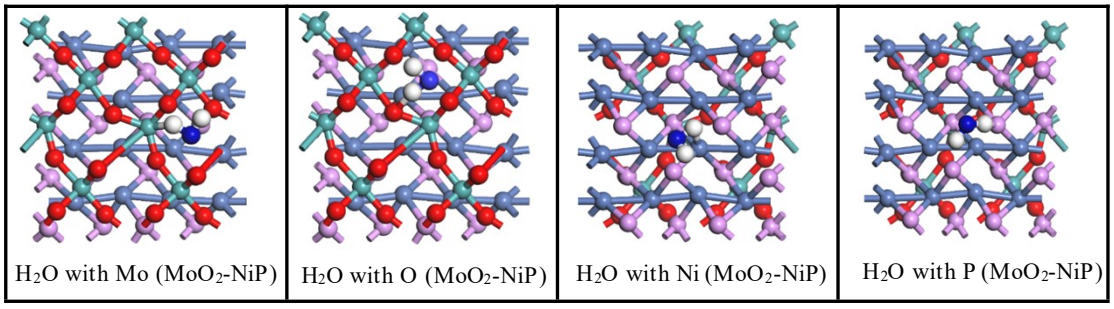

Figure S8. Water molecule adsorption models on different adsorption sites (Ni, Mo, O, P). Colors represent the following atoms: red (O from the surface), dark blue (O from the water molecule), cyan (Mo), pink (P), light blue (Ni), and white (H).

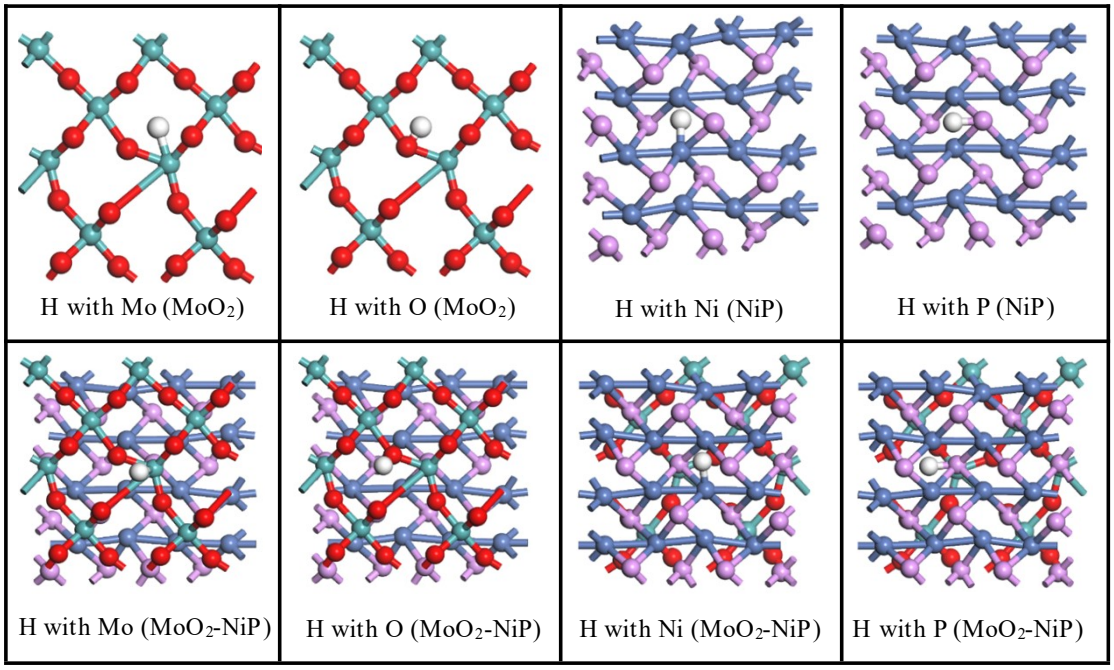

Figure S9. H atom adsorption models on different adsorption sites (Ni, Mo, O, P). Colors represent the following atoms: white (H), light blue (Ni), cyan (Mo), red (O), and pink (P).

Table S1. The mass ratios of NiP to MoO_2 in MoO_2-NiP/NF-300, MoO_2-NiP/NF-400, and MoO_2-NiP/NF-500.

Mass percentage (wt.%)	NiP/MoO_2
300°C	0.48
400°C	0.87
500°C	1.78

Table S2. Comparison of HER activities of MoO_2-NiP/NF-400 with recent reported metal phosphides catalysts in 1 M KOH.

Catalysts	Overpotential @ 10 mA cm^{-2} (mV)	Tafel slope (mV dec^{-1})	References
MoO_2-NiP/NF-400	19	22.18	**This work**
MoC-Mo_2C	114	62	[1]
NiS_2/CoS_2/MoS_2	112	59	[2]

Fe-NiMo alloy	28	33.92	[3]
Fe-CoP-1	85	68.7	[4]
CNSC/NF	80	65	[5]
CN/CNL/MoS_2/CP	106	117	[6]
Ni-Mo-P/NF	53	47.18	[7]
N-MoS_2/AOCF-C	166	48.83	[8]
CoS_2/MoS_2@CC	71	62.8	[9]
NiO@NF-16	109	103.9	[10]
Cu-CoS_x/NF	75	64.6	[11]
Mo-Ni_3S_2	144	68.47	[12]

References

1. W. Liu, X. Wang, F. Wang, K. Du, Z. Zhang, Y. Guo, H. Yin and D. Wang, *Nat. Commun*, 2021, **12**, 6776.
2. Y. Zhang, M. Shi, C. Wang, Y. Zhu, N. Li, X. Pu, A. Yu and J. Zhai, *Sci. Bull*, 2020, **65**, 359-366.
3. B. Zhao, M. Chen, J. Zhang, H. Sun, B. Zhao, D. Li, Y. Wu, T. Zhou, F. Liu, H. Cui and Q. Liu, *Chem. Eng. J*, 2026, **536**, 175938.
4. P. Zhou, Z. Li, Y. Zhang, H. Zhang, M. Zhang, D. Han and X. Chen, *Int. J. Hydrogen Energy*, 2025, **145**, 139-146.
5. F. Jiang, Y. Wang, H. Peng, Y. Wu, Z. Zhang, Y. Li, S. Zhong, X. Chen, J. Li, Y. Wang, J. Peng and M. Zhai, *Appl. Catal. B: Environ. Energy*, 2025, **372**, 125326.
6. J. Dong, X. Zhang, J. Huang, J. Hu, Z. Chen and Y. Lai, *Chem. Eng. J*, 2021, **412**, 128556.
7. Y. Wei, T. Yu, H. Zhao, X. Wu, L. Sun and S. Mu, *Int. J. Hydrogen Energy*, 2026, **235**, 155137.
8. X. Lu, T. Tao, Y. Zhang, S. Lu, J. Xie, Z. Ding and Z. Wu, *ChemistrySelect*, 2023, **8**, e202204699.
9. G. Zhou, X. Wu, M. Zhao, H. Pang, L. Xu, J. Yang and Y. Tang, *ChemSusChem*, 2021, **14**, 699-708.
10. I. A. Poimenidis, M. Lykaki, S. Moustaizis, P. Loukakos and M. Konsolakis, *Mater. Chem. Phys*, 2023, **305**, 128007.
11. H. He, L. Zeng, X. Peng, Z. Liu, D. Wang, B. Yang, Z. Li, L. Lei, S. Wang and Y. Hou, *Chem. Eng. J*, 2023, **451**, 138628.
12. J. Li, X. Meng, X. Qi and Y. Fang, *J. Electroanal. Chem*, 2026, **1012**, 120103.